ACS OMEGA

Open Access

http://pubs.acs.org/journal/acsodf

Article

Predicting the Decomposition Mechanism of the Serine α-Amino Acid in the Gas Phase and Condensed Media

Mubarak Al-Kwradi, Labeeb Ali, and Mohammednoor Altarawneh*

Cite This: *ACS Omega* 2024, 9, 8574−8584

Read Online

ACCESS | Metrics & More | Article Recommendations | Supporting Information

ABSTRACT: Comprehending the nitrogen combustion chemistry during the thermal treatment of biomass demands acquiring a detailed mechanism for reaction pathways that dictate the degradation of amino acids. Serine (Ser) is an important α-amino acid that invariably exists in various categories of biomass, most notably algae. Based on density functional theory (DFT) coupled with kinetic modeling, this study presents a mechanistic overview of reactions that govern the fragmentation of the Ser compound in the gas phase as well as in the crystalline form. Thermokinetic parameters are computed for a large set of reactions and involved species. The initial decomposition of Ser is solely controlled by a dehydration channel that leads to the formation of a 2-aminoacrylic acid molecule. Decarboxylation and deamination routes are likely to be of negligible importance. The falloff window of the dehydration channel extends until the atmospheric pressure. Bimolecular reactions between two Ser compounds simulate the widely discussed cross-linking reactions that prevail in the condensed medium. It is demonstrated that the formation of the key experimentally observed products (NH_3, CO_2, and CO) may originate from direct bond fissions in the melted phase of Ser prior to evaporation. A constructed kinetic model (with 24 reactions) accounts for the primary steps in the degradation of the Ser molecule in the gas phase. These steps include dehydration, decarboxylation, deamination, and others. The kinetic model presents an onset decomposition temperature of 700 K with the complete conversion attained at ∼1090 K. Likewise, the model portrays the temperature-dependent increasing yields of CO_2 and NH_3. The results presented in this work offer a detailed analysis of the intricate chemical processes involved in nitrogen transformations, specifically in relation to amino acids. Amino acids play a crucial role as the primary nitrogen carriers in biomass, such as microalgae and protein-rich biomass.

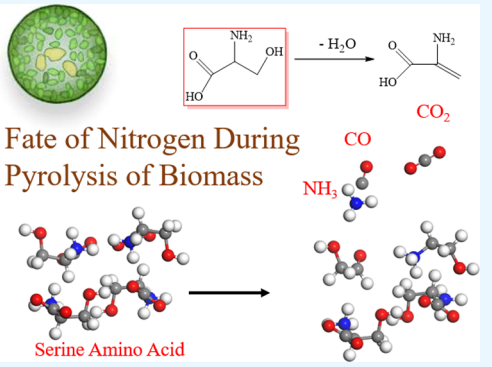

1. INTRODUCTION

Pyrolysis and combustion constitute the most viable strategies for the industrial-scale utilization of biomass as a source of liquid bio-oil.[1] However, in addition to hydrocarbon streams, these processes convert the oxygen and nitrogen contents in biomass into a large array of O- and N-containing pollutants.[2] The latter spans the notorious nitrogen oxides NO*x*; HCN, NH_3, HNCO, alkyl amines; and N-polyaromatic hydrocarbons (N-PAHs such as carbazole and phenazine).[3−5] The emission intensity of these species truly stems from the nitrogen transformation chemistry during the thermal treatment of biomass.[6] The building structures of nitrogen in biomass differ from that of other fuels, such as coal (where nitrogen is mainly incorporated in 6- and 5-ring structures).[7] Hence, the synthesis of N-species ensues via distinct pathways in biomass that are sensitive to their nitrogenated fragments. It is generally viewed that the high O/N ratios in biomass promote the conversion of the nitrogen content into N-volatile entities.[7] However, the formation of nitrogenated species from the pyrolysis of biomass also involves complex multiphase reactions where interactions with char and the appreciable mineral contents play a major role. The relative distribution of N-species in volatile and char fractions depends on many factors such as heating rates, deployed reactor's type, and particle's size. Leng et al.[8] comprehensively surveyed features that affect the yield of N-compounds in bio-oil, with a prime focus on biomass makeup and biochemical and mineral compositions.

Nitrogen in biomass does not exist as aromatic heterocyclic structures but rather as an N-protein that usually accounts for ∼85% of the total nitrogen content in biomass.[9] Amino acids are the building blocks in N-protein.[8] In reference to the commonly deployed *N*-alkyl amines (such as dimethylamine and ethylamine) and heterocycles (such as morpholine), amino acids serve as representative model compounds of real samples of biomass.[10] For this reason, several studies investigated the thermal decomposition of selected amino acids as an important milestone in comprehending the chemistry of nitrogen during the thermal utilization of

Received: December 29, 2023
Revised: January 16, 2024
Accepted: January 22, 2024
Published: February 6, 2024

biomass.[11] There are 20 types of amino acids with structures as simple as glycine and as complex as tryptophan. A survey by Ren and Zhao[12] reported the composition of amino acids in various types of Wheat straw and Corn cob. It was found that certain amino acids such as serine and aspartic acid exist in appreciable concentrations in the range of 1.0−3.3 mg/g. As such, amino acids (i.e., N-protein) serve as representative candidates to formulate the mechanistic pathways that dictate the emission of N-species from the thermal treatment of biomass.

Removal or reducing the nitrogen content (denitrogenation) in biomass is an essential step in the production of biofuel.[13] Central to this step is to acquire a detailed understanding of chemical reactions that dictate the decomposition of amino acids and subsequent emission of N-species. Thermal-induced fragmentation of amino acids is rather a complex process in which the formation of the major N-carriers (such as NH_3 and HCN) may originate reactions that involve secondary products and intermediates; i.e., not as initial products of pyrolysis.[14] Primary exit channels for amino acids span dehydration into cyclic amides (i.e., diketopiperazine DKP), decarboxylation into amines, and deamination.[15] The relative importance of these initial reactions differs from one type of biomass to another. For instance, deamination reactions are prominent in the case of energy crops and lignocellulose when compared to sludge and microalgae. We have illustrated in a previous study that the formation of the experimentally major observed products from pyrolysis of leucine amino acid takes place via bimolecular reactions.[16] Such reactions typically occur in the condensed medium prior to evaporation. The relevance of bimolecular reactions becomes more profound in view of the very high boiling points of amino acids (i.e., the boiling temperature of serine at 1.0 atm is ∼400 °C).[17] Following the initial reactions, a complex network of reactions evolves to generate amines, nitriles, α-lactam, and pyrroline. Secondary fragmentation reactions of imine and amine mainly produce NH_3 and alkyl diamine.[18] Cracking reactions of N-bounded char produce HCN and HCNO. Formulated mechanisms were guided by online measurements of evolved products either offline or via online TG-IR-MS sampling.[19,20]

In microwave pyrolysis of certain amino acids (namely, serine, phenylalanine, and glutamic acid), the selective formation of N-compounds displays sensitivity to temperature, whereas the low-temperature window (i.e., 300 °C) favored the generation of amines and cyclic amides through the aforementioned three primary channels.[21] Higher temperatures (400−500 °C) converted amines and amides into nitriles (such as propionitrile) and N-heterocycle (such as pyrrole and indole). In the case of serine amino acid, in particular, the nitrogen content displayed a profound tendency to accumulate in the bio-oil when (i.e., ∼15% at 500 °C) compared with other amino acids (3−10% at 500 °C). Evolved gases from the decomposition of the serine model mainly constituted CO, CO_2, NH_3, and HCN. Formation of these products indicates the occurrence of decarbonylation, decarboxylation, deamination, and secondary cracking reactions, respectively.[19] The formation of N-heterocycles from pyrolysis of amino acids stems from Maillard-type reactions.[22] Sato and colleagues[23] conducted a thorough analysis using a continuous flow tubular reactor to explore the decomposition reactions of five distinct amino acid models: alanine, leucine, phenylalanine, serine, and aspartic acid. This experiment was carried out under specific conditions involving temperatures ranging from 200 to 340 °C, pressure at 20 MPa, and reaction times varying from 20 to 180 s. Their findings highlighted that, within these specified conditions, the primary reaction pathways included deamination, resulting in the formation of organic acids and ammonia, as well as decarboxylation, which produced amines and CO_2. The deamination and decarboxylation reactions were found to be significant for the amino acid models. Notably, in the case of alanine, the decomposition process proceeded via lactic acid and pyruvic acid intermediates, ultimately releasing carbon dioxide. For aspartic acid, deamination was the dominant reaction, while serine underwent decomposition to yield glycine and alanine. By employing a first-order kinetics framework, it was determined that the degradation rates of the considered amino acids follow the order aspartic acid > serine > phenylalanine > leucine > alanine.[23] However, it is essential to acknowledge that the study's utilization of very short residence times limits its direct applicability to the field of microalgae liquefaction, which typically occurs over extended timeframes.[23]

Despite recent progress in revealing the complex reaction mechanisms that govern the fragmentation of amino acids through combined pyrolytic experiments and molecular modeling, prominent mechanistic features remain largely speculative. The most intriguing questions pertain to energy requirements of the primary reactions, the fate of the initially formed intermediates, and the potential importance of bimolecular reactions in the condensed melted medium prior to evaporation.

To this end, the aim of this study is to explore reactions that operate in the pyrolysis of serine (Ser) amino acid compound. The unique structure of the Ser compound features the presence of adjacent amine, hydroxyl, and carbonyl groups. As such, the acquired mechanisms in this work are also applicable to more sophisticated amino acids that contain these functional groups. The aim of this contribution is 3-fold: to present reaction pathways that underpin the initial decomposition of the Ser compound, to compute energy requirement for the self-reaction of Ser molecules, and to formulate a reduced kinetic model that accounts for the decomposition of Ser molecules in the gas phase. An important part of this work also investigates the occurrence of deamination and decarboxylation reactions in the condensed melted phase as primary sources for the experimentally observed NH_3 and CO_2 molecules. It is hoped that the work presented herein will be useful in the overall pursuit of reducing nitrogen content in bio-oil.

2. COMPUTATIONAL METHODOLOGIES

Herein, we have deployed a multitude of computational tools to investigate the decomposition of the Ser compound in the gas phase as well as in the condensed phase. Figure 1 portrays the computer codes utilized and their corresponding outputs. The Gaussian 16 code[24] computes potential energy surfaces (PES) for the unimolecular and bimolecular reactions that operate in the degradation of the Ser molecule in the gas phase based on the CBS-QB3[25] composite chemistry model. This composite model has been devised to achieve a high level of chemical precision in more extensive systems. The CBS-QB3 model performs several single-point energy calculations at high theoretical levels (CCSD(T)/6-31 + G(d′); MP4SDQ/CBSB4; MP2/CBSB3) on preoptimized structures at the B3LYP/CBSB7 level of theory. It is well established that the CBS-QB3 method provides satisfactory performance in

https://doi.org/10.1021/acsomega.3c10496
ACS Omega 2024, 9, 8574−8584

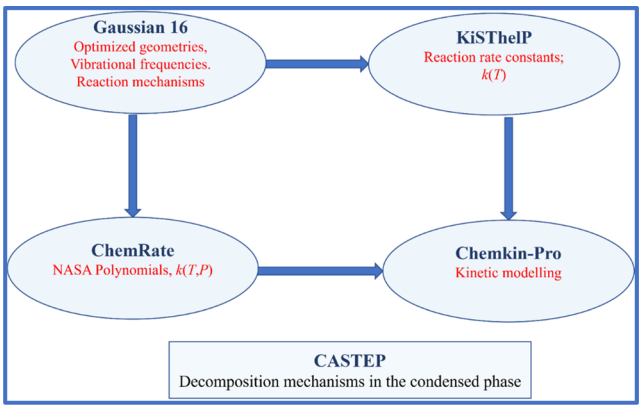

Figure 1. Deployed computer codes in this work and their utilizations.

deriving thermokinetic parameters for general applications in the chemistry of hydrocarbons.[26,27] For instance, in a previous study,[28] we demonstrated the activation and reaction energies for selected RH + NH_2 reactions, computed by the CBS-QB3 method, to incur mean unsigned errors of 1.48 and 2.94 kJ mol/mol, respectively, in reference to analogous values computed by the G4 method. Likewise, our computed reaction enthalpies for selected amines + NH_2 reactions were found to reside within 1−2 kJ/mol from analogous ATcT-derived values.[29] The seminal work by Simmie's group[30] on the thermochemistry of hydrocarbon radicals established a relatively satisfactory performance of CBS-QB3 when compared with other more computationally expensive models. IRC calculations were used to connect the transition states with their corresponding reactants and products along the designated reaction pathway.

Upon the determination of minimum energy points along the specified reaction coordinates, reaction rate constants were computed using the KiSThelP[31] based on the conventional TST, with the inclusion of a Wigner's correction for plausible tunneling effects. Based on calculated vibrational frequencies, rotational constants, and standard enthalpies of formation, the ChemRate code[32] derives temperature-dependent thermochemical properties in the form of NASA polynomials that are required in kinetic modeling. In these computations, we account for the internal rotations of various groups (C−H, N−H, and O−H) in the case of the Ser molecule and its resulting products, treating them as hindered rotors. The utilization of this approach and its influence on attaining accurate thermochemical data has been detailed in the literature.[33] Essentially, this technique entails partially optimizing the system by systematically scanning dihedral angles at 30° intervals, assessing the rotational barriers, computing moments of inertia for the rotor components, and determining their rotational symmetry numbers. The treatment of hindered rotors in the KiSThelP is based on the McClurg et al.[34] method that only utilizes the overall rotational barrier associated with the assigned harmonic frequency. The ChemRate code also calculated $k(T,P)$ for important unimolecular reactions based on the Rice−Ramsperger−Kassel−Marcus (RRKM) theory.[35] We carried out kinetic modeling of the Chemkin-Pro package based on a CSTR model while deploying a residence time of 1 s.

Finally, the CASTEP code[36] is used to simulate the degradation of the Ser compound in the condensed medium (i.e., crystalline form) according to the GGA-PBE method.[37] The computational methodology comprises the use of 2 × 2 unit cells of the condensed Ser compound, a 2 × 2 × 1 κ-point sampling, a cutoff energy at 300 eV, and the "on-the-fly" pseudopotential. More details on the applied methodologies and accuracy benchmarking can be found in other studies.[38−41] Figure 1 portrays the computational framework deployed in this work and the connections between the various tasks and their respective codes. For instance, vibrational frequencies and rotational constants were computed from the Gaussian 16 code and then used as input into the ChemRate code to derive NASA polynomials. Calculated reaction rate constants from KisThelP together with NASA polynomials are then utilized to formulate the kinetic model. Tables S1−S29 (Supporting Information, SI) list the Cartesian coordinates and vibrational frequencies for all optimized structures. Scheme S1 in the SI

Scheme 1. Isodesmic Reactions to Calculate the Standard Enthalpy of Formation of the Ser Molecule (Values Are in kJ/mol)[a]

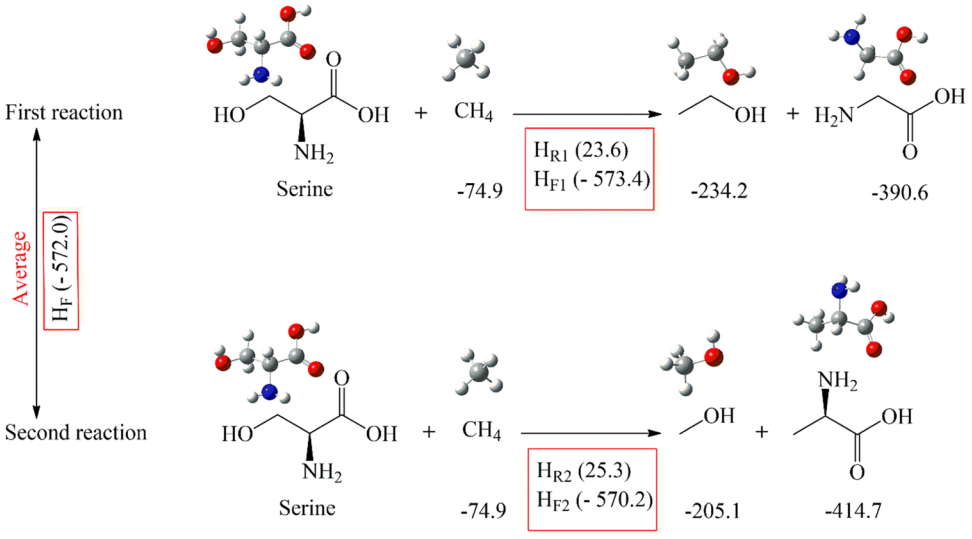

[a]Utilized experimental enthalpies of formation of the reference species are shown in the scheme.

https://doi.org/10.1021/acsomega.3c10496
ACS Omega 2024, 9, 8574−8584

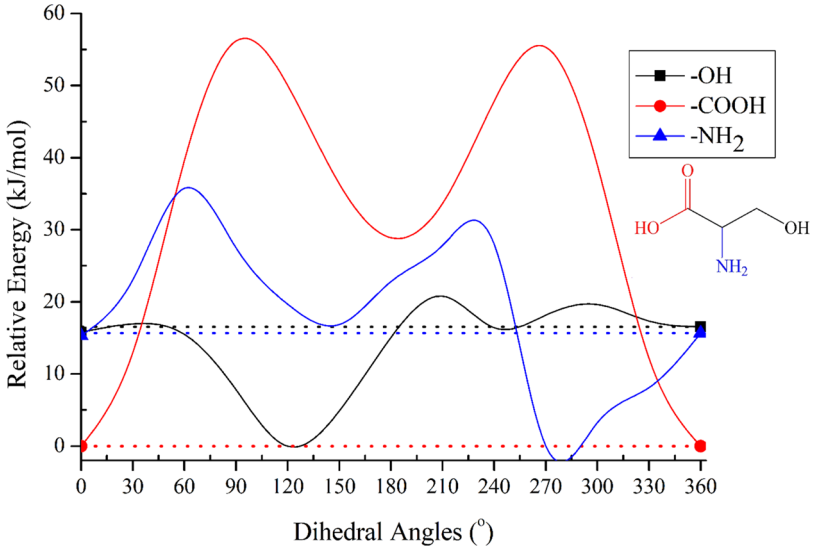

Figure 2. Relaxed potential energy profiles for the internal rotations in the Ser molecule calculated at the hybrid-metal M062X/6-31+G(d) level of theory. The energy scan involves the four atoms that characterize the dihedral angles of the corresponding functional groups. Values of energy for each rotational curve are calculated in reference to the minimum energy point for their corresponding rotations.

Table 1. Computationally Calculated Thermochemical Properties of Selected Compounds and Intermediates

compound	ΔH_{f298}° (kJ/mol)	$S_{298.15}^{\circ}$ (J/mol. K)	C_p (300 K) (J/mol. K)	C_p (500 K) (J/mol. K)	C_p (800 K) (J/mol. K)	C_p (1000 K) (J/mol. K)
Serine	−570.2	459.3	150.8	204.9	255.5	276.4
P1	−358.3	428.9	139.0	187.2	233.1	252.6
P2	−396.8	451.9	145.8	197.9	244.8	263.4
P3	−490.8	451.3	150.9	198.9	241.9	260.0
P4	−398.1	457.3	151.7	200.6	243.9	261.8
P5	−378.7	426.5	138.8	187.9	232.5	251.5
M1	−319.4	380.8	120.1	162.3	199.9	215.8
M2	−225.0	354.3	100.7	141.4	181.5	198.6
M3	−515.8	381.5	108.8	144.8	178.1	191.6
M4	−64.0	365.5	102.9	138.1	172.8	187.7
M5	−295.1	356.8	106.8	138.4	167.1	179.2

document lists the parameters and general governing equations of the computational workflow.

3. RESULTS AND DISCUSSION

3.1. Thermochemistry. To the best of our knowledge, the literature presents no value for the standard enthalpy of formation of the gas-phase ($\Delta H_{f298.15}^{\circ}$) Ser molecule, presumably due to its very high boiling point at ∼394 °C. Scheme 1 presents the two utilized isodesmic reactions, from which the average $\Delta H_{f298.15}^{\circ}$ for the serine compound was evaluated to be −572.0 kJ/mol.

This isodesmic reaction preserves the type and number of bonds across the two sides of the reaction. Enthalpies of the formation for the three deployed reference species were sourced from the NIST online database (https://webbook.nist.gov/chemistry/)[42] based on their original experimental references.[43−45] Enthalpies of formation for derived products from the unimolecular and bimolecular reactions involving Ser were computed based on the obtained $\Delta H_{f298.15}^{\circ}$ of the Ser compound. Moreover, the relaxed potential energy profile for Ser molecules and their derivatives relates to the changes in energy that occur as a specific bond's dihedral angle within the molecule undergoes rotation. More specifically, it focuses on the rotational behavior of a particular bond within the Ser molecule and examines the corresponding variations in energy.

Figure 2 depicts the energy potential profiles for the Ser molecule, illustrating the rotation of amino hydrogen atoms around different bonds such as C═O, O−H, and N−H. For example, the associated barrier for the internal rotation about the O═C−O−H dihedral angle in Ser is measured at 58.0 kJ/mol, which closely aligns with the reported experimental value of alanine amino acid by 54 kJ/mol.[46] The majority of rotational profiles in other Ser-derived product compounds feature 2-fold rotors with characteristic peaks, while some profiles exhibit 1-fold and 3-fold rotors.

In addition to values of $\Delta H_{f298.15}^{\circ}$ for the various species considered herein, Table 1 enlists standard entropies and heat capacities at selected temperatures after treatment, while the SI document shows the difference between treatment and nontreatment results (Table S30).

Figure 3 presents all possible direct bond dissociation enthalpies (BDHs) in the Ser compound. In our recent study on the bimolecular reactions of Ser with selected radicals,[47] we demonstrated that the α C−H bond incurs the lowest C−H BDHs at 298.8.0 kJ/mol (P3 + H) followed by fission of the secondary C−H and N−H bonds at ∼392 kJ/mol. Fission of the secondary C−H bond liberates P1 + H + CO_2 fragments.

As Figure 3 shows, the secession of the C−COH bond entails the lowest BDHs in the thermal decomposition of the Ser compound at only 271.4 kJ/mol (Ser → M5; OH−C(O)−

https://doi.org/10.1021/acsomega.3c10496
ACS Omega 2024, 9, 8574−8584

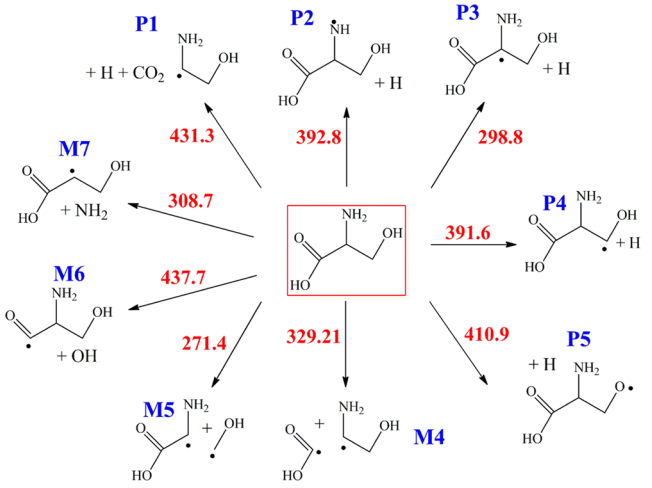

Figure 3. Bond dissociation enthalpies (BDHs) in the Ser molecule. All values are in kilojoules per mole computed at 298.15 K.

$CHNH_2$ + CH_2OH), significantly weaker than the α C−H bond at 298.8 kJ/mol. Thus, prior to the establishment of the O/H/N radical pool, the fission of this bond may play a central role in the fragmentation of the Ser compound. The presence of the NH_2 electron-donating group appears to weaken the C−H_2COH in reference to the analogous C−H_2COH bonds in linear and branched alkanes whose BDHs generally reside between 350 and 360 kJ/mol, as in propanol at 355 kJ/mol.[47]

3.2. Unimolecular Decomposition Pathways. Unimolecular fragmentation routes of amino acids often feature hydration, decarboxylation, and deamination pathways.[23] In the case of leucine, for instance, activation barriers for these three pathways reside between 280 and 300 kJ/mol. Figure 4 portrays energy requirements for the three pathways mentioned above for the Ser compound. Activation enthalpy for the dehydration pathway amounts to 220.9 kJ/mol via the transition state TSM1. The latter resembles a three-centered transition state in which a water molecule is eliminated through the combustion of the outer hydroxyl group with the α H atom (Scheme 2).

A relatively low activation enthalpy of TSM1 stems from a weak α−C−H bond (298.8 kJ/mol). The dehydration channel

Scheme 2. Geometries of TSM1, the Dehydration Channel as an Example[a]

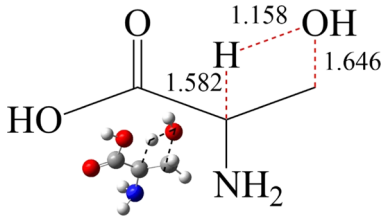

[a]Distances are in Angstrom Å.

is slightly endothermic at 8.8 kJ/mol and results in the formation of 2-aminoacrylic acid (M1). In living tissues, the presence of 2-aminoacrylic acid often serves as a sign of aging-related diseases[48] and is postulated to form via uncatalyzed post-translational reactions between Ser and cysteine.[49] Likewise, 2-aminoacrylic acid is a common product from the hydrothermal cracking of amino acids and forms through intra- and intermolecular protein cross-linking accompanied by water elimination.[50] This general hypothesized mechanism is in line with the dehydration channel shown in Figure 4. The importance of the water elimination channel was also highlighted in recent studies that investigate the chemistry underlying the formation of peptide bonds in the energetic processing of amino acids.[51−53]

The effect of the pressure on the kinetics of the dehydration channel using RRKM theory as implemented in the ChemRate code is studied for this channel. In the calculations of $k(T,P)$ values of the dehydration route, Lennard-Jones parameters of acetamide[54] were used while utilizing an exponential-down model with ΔE_{down} at 250 cm^{-1} to simulate moderate collision conditions. As Figure 5 shows, the falloff region extends nearly until the atmospheric pressure and the k(900 K, 1 atm) deviate from the corresponding high-pressure limit by a factor of ∼0.1.

The decarboxylation and deamination channels entail activation barriers of 282.1 (TSM2) and 273.9 kJ/mol (TSM3), respectively. These values are in accord with analogous values previously computed for leucine at 299.5 and 278.8 kJ/mol, respectively, computed at the CBS-QB3.[16] It is unlikely that these two channels will significantly participate in the initial degradation of the Ser compound.

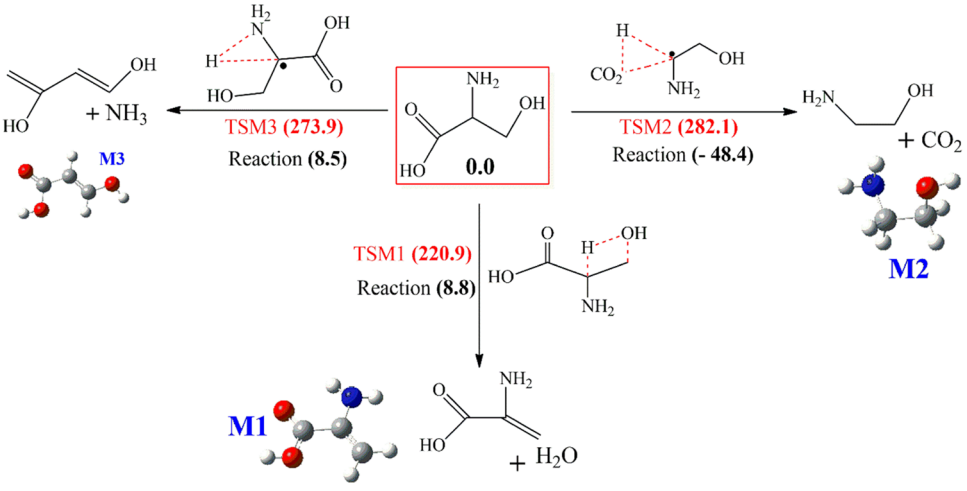

Figure 4. Reaction and activation enthalpies for the three initial exit pathways of the serine molecule: dehydration, deamination, and decarboxylation. All values are in kJ/mol computed at 298.15 K.

https://doi.org/10.1021/acsomega.3c10496
ACS Omega 2024, 9, 8574−8584

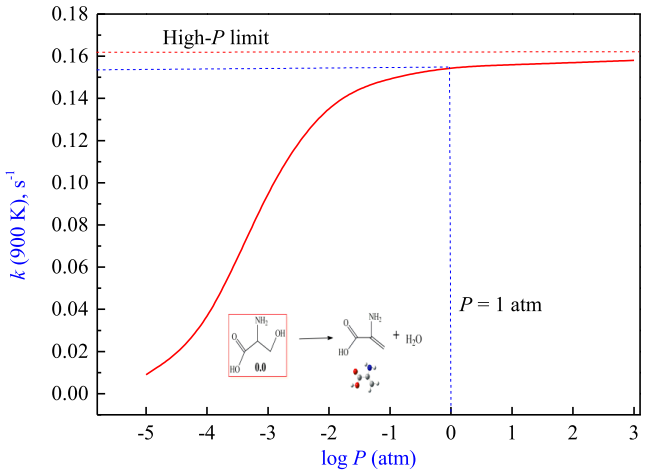

Figure 5. Effect of pressure on the reaction rate constant for the dehydration channel serine → H_2O + 2-aminoacrylic acid reaction at 900 K. The upper dashed line denotes the high-P limit.

The calculated barrier for the decarboxylation channel (282.1 kJ/mol) is significantly lower than the corresponding free-energy barrier of the decarboxylation value computed by Xu et al.[21] at the B3LYP/6-311G level of theory (328.0 kJ/mol). Such a difference arises from the well-documented inaccuracy of the B3LYP method in the estimation of reaction barriers.[55] Most importantly, the study by Xu et al.[21] did not identify the lowest-energy pathway pertinent to the dehydration channel.

3.3. Radical-Prompted Pathways. Abstraction of a H atom from the various sites in the Ser compound ensues via accessible enthalpic barriers.[47] Thus, it is anticipated that in the gas phase, the decomposition of the Ser molecule will take place solely via radical-derived pathways. Figure 6 shows detailed degradation pathways for the P2−P5 radicals that form following the loss of a H atom from the Ser molecule. The P3 radical for instance emerges from the abstraction of the α C−H atom, while the P4 radical forms after the expulsion of a H atom from the secondary site. Likewise, P2 and P5 radicals stem from the removal of a H atom from the amine and hydroxyl radicals, respectively. The upper part of Figure 6 shows decarboxylation routes that start from the P3 and P4 radicals through activation enthalpies of 193.2 (TSR1) and 61.3 kJ/mol (TSR2), respectively. In addition to CO_2, these two reactions form the M4 adduct (NH_2CHCH_2OH). The latter decomposes via barrierless channels into the CH_2OH radical and $^+NH_2CH$ (methylene, 1-amino) and OH and H_2NCHCH_2 (ethenamine). The latter channel is endothermic by 110.9 kJ/mol, while the former is endothermic by 390.2 kJ/mol. While the formation of ethenamine is thermodynamically endothermic, this channel also produces the chain propagating radicals OH.

The lower part of Figure 6 shows that the formation of the formaldehyde and the M5 intermediate from the degradation

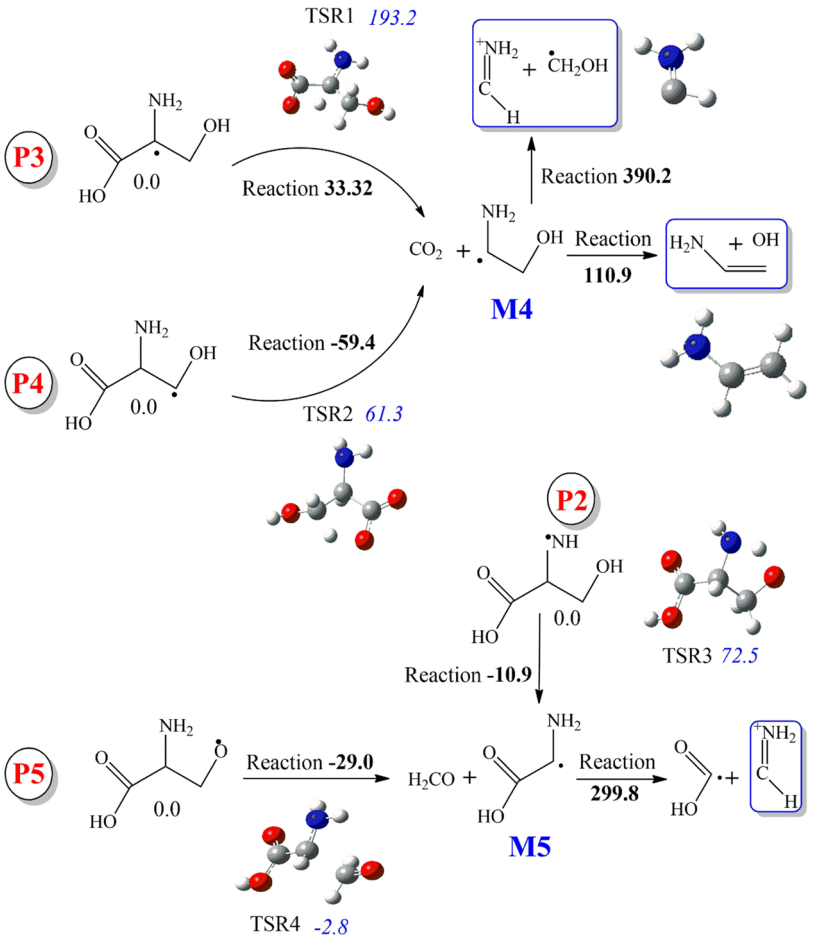

Figure 6. Reaction pathways that operate in the decomposition of the initial radicals that form after the loss of a H atom from the serine molecule. Values are given in kJ/mol at 298.15 K.

https://doi.org/10.1021/acsomega.3c10496
ACS Omega 2024, 9, 8574−8584

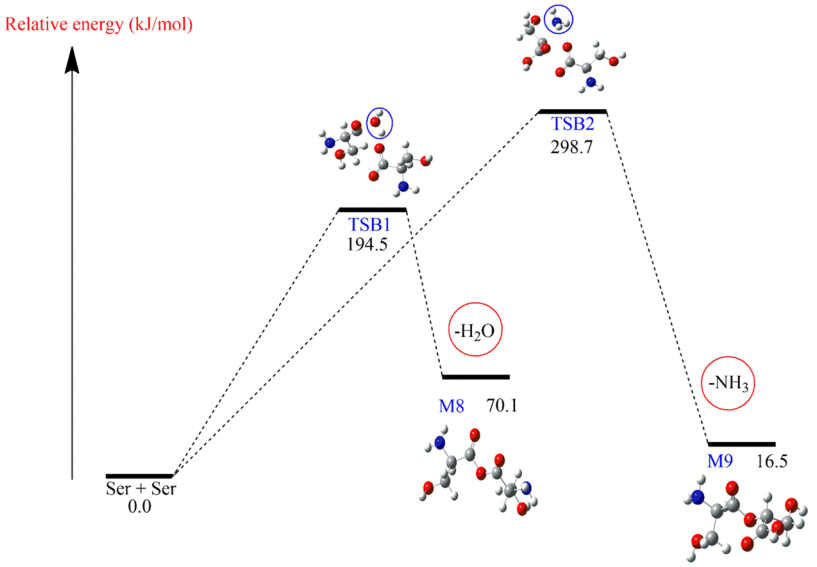

Figure 7. Enthalpic energy profile for the self-reaction (bimolecular) of the serine molecules.

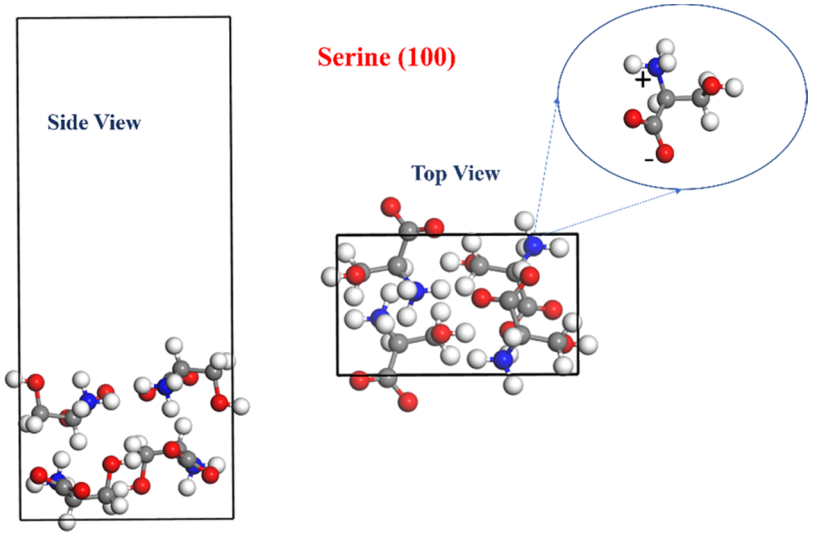

Figure 8. Optimized "serine" surface terminated along the [100] direction. Blue, red, white, and gray spheres denote N, O, H, and C atoms, respectively.

of P2 and P5 radicals either take place via facile activation enthalpy of 72.5 kJ/mol (TSR3) and −2.8 kJ/mol (TSR4), which indicates a barrierless reaction, and the reaction rate is proportional to the collision frequency[56] (barrierless pathways). Further degradation of the M5 moiety produces methylene, 1-amino, and the OH(CO) radical in a noticeably endothermic reaction of 299.8 kJ/mol.

3.4. Self-Condensation of Ser Compounds. Decomposition of amino acids in their condensed medium (as in the case of other biomass constituents) is governed by cross-linking reactions between adjacent entities.[57] The very high boiling point of amino acids, in general, further enhances the contribution of the cross-linking reaction in the condensed medium prior to evaporation of the fragmented entities. To simulate these chemical phenomena, Figure 7 plots the thermodynamic profile for Ser bimolecular reactions where two channels are characterized. The first reaction pathway signifies the elimination of a water molecule, leading to the formation of the M8 adduct. This reaction demands an accessible activation enthalpy of only 194.5 kJ/mol through transition state TSB1. The low barrier of this transition state reconciles with TGA profiles of the condensed Ser that typically commences around ∼230 °C.[21] The water elimination channel is endothermic by 70.1 kJ/mol. As demonstrated by Chen et al.,[19] the initial decomposition of amino acids (such as aspartic and glutamic acids) takes place via intramolecular dehydration routes. While we have not investigated further degradation of the M8 intermediate, its further fragmentation may lead to the synthesis of the experimentally[21] observed products in the Ser's bio-oil such as pyrazine and pyrrole. Xu et al.[21] proposed pathways for the formation of the two latter compounds from unimolecular arrangements of the parent Ser compounds, but despite our best efforts, we were unable to reproduce these pathways. The deamination route through transition state TSB2 (298.7 kJ/mol) is likely to be inhibited when compared with the dehydration route.

https://doi.org/10.1021/acsomega.3c10496
ACS Omega 2024, 9, 8574−8584

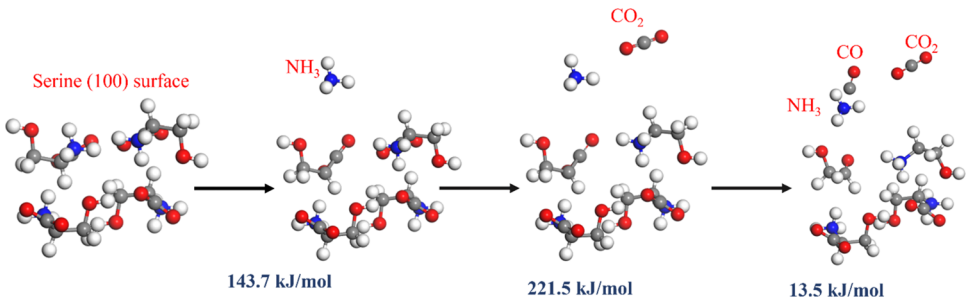

Figure 9. Thermodynamic profile for the emission of NH_3, CO_2, and CO from the decomposition of a surface model of serine. For clarity, the boundaries of the surface model have been removed.

3.5. Decomposition of Ser in the Condensed Medium. Accurate description of the decomposition of amino acids during pyrolysis of biomass demands a study of their fragmentation in the condensed medium. For this reason, we report herein the initial steps that dictate the emission of the primary products from the decomposition of Ser (namely, NH_3, CO_2, and CO[21]) based on a solid state unit cell model. The unit cell of Ser was sourced from a study by Moggach et al.[58] Figure 8 shows the optimized structure (using the CASTEP code) of crystalline Ser truncated along the [100] direction. The Ser building blocks exist in the ionic form. This facilitates the direct expulsion of NH_3 and CO_2 as Figure 9 shows. The energy trend presented in Figure 9 is in qualitative agreement with the experimental results reported by Xu et al.[21] NH_3 signifies the major nitrogen carrier from the fragmentation of Ser. Formation of ammonia takes place via the fission of a C-NH_3 bond in a process that demands only 143.7 kJ/mol without encountering an intrinsic reaction barrier. Thus, it is anticipated that while the gas-phase deamination route is of negligible importance, the formation of ammonia occurs through direct bond fission in the crystalline phase. The low-energy requirement for ammonia emission is also in line with the reported onset temperature for the decomposition of Ser at 230 °C.[21]

The concentration of CO_2 from the degradation of Ser peaked at 30% (300 °C).[21] CO_2 is formed through the fission of C−CO_2 in crystalline Ser in a reaction that requires 221.5 kJ/mol of energy. Thus, we envisage that CO_2 does not form through a decarboxylation step as demonstrated by Xu et al.[21] In the final step, a CO molecule forms via a trivial endothermicity of 13.5 kJ/mol. The other major product, HCN most likely originates from the combustion cycle of nitrogen that involves complex reactions of ammonia and hydrocarbon entities.

3.6. Kinetic Modeling for the Decomposition in the Gas Phase. Computed thermokinetic parameters are utilized to construct a detailed kinetic model to account for the decomposition of the Ser compound in the gas phase. Table 2 lists calculated Arrhenius parameters for the gas-phase reactions covered in previous sections. A CSTR reactor model is used at a residence time of 1.0 s. Such a relatively long residence time has been considered to further facilitate the potential occurrence of bimolecular reactions; however, considering shorter residence times (at 0.5 and 2 s) did not significantly change the decomposition profiles. The inlet feed consisted of 5% Ser diluted in 95% N_2. The model comprises 26 species and 24 reactions. Kinetic modeling was carried out between 500 and 1500 °C at 1 atm. Figure 10 plots the conversion of Ser in the gas phase and temperature-dependent profiles of key products.

Table 2. Computed Reaction Rate Parameters That Are Deployed in the Kinetic Model

reaction	A (cm^3/mol·s)	E_a (kJ/mol)
Ser → H_2O + M1	3.47×10^{13}	230.3
Ser → CO_2 + M2	3.40×10^{13}	276.3
Ser → NH_3+ M3	2.64×10^{13}	268.0
Ser → H + P3	1.00×10^{14}	299.0
Ser + H → H_2 + P3	1.11×10^{13}	21.8
Ser + OH → H_2O + P3	1.56×10^{12}	2.9
P3 → CO_2 + M4	3.82×10^{12}	33.5
M4 → OH + C_2H_3N	1.00×10^{13}	111.0
Ser + H → CO_2 + H_2 + M4	5.27×10^{13}	52.3
Ser + H → H_2 + P4	2.23×10^{13}	23.4
Ser + H → H_2 + P5	2.36×10^{13}	49.0
Ser + H → H_2 + P2	3.32×10^{12}	30.1
P4 → CO_2 + M4	2.11×10^{12}	0.0
P5 → CH_2O + M5	9.61×10^{12}	0.0
P2 → CH_2O + M5	6.84×10^{12}	0.0
M5 → $HCNH_2$ + HOCO	1.00×10^{13}	464.8
Ser + OH → H_2O + P4	1.50×10^{11}	0.0
Ser + OH → H_2O + P5	1.56×10^{12}	22.6
Ser + Ser → H_2O + M8	3.34×10^{10}	194.7

As Figure 10a shows, the decay of the Ser compound commences at 700 K and a complete conversion is attained at ∼1090 K (at a residence time of 1.0 s). As expected, utilizing shorter (0.5 s) and longer (2.0 s) residence times causes conversion to commence at slightly lower and higher onset temperatures, respectively, as Figure 10a portrays. Normalized sensitivity analysis reveals that Ser solely decomposes via H_2O + 2-aminoacrylic acid with no noticeable contribution from other unimolecular or bimolecular routes at all temperatures. 2-Aminoacrylic acid signifies the most important predicted product with a relative yield of 0.9 at 1100 K (Figure 10b). Ethynamine (Figure 10c) appears in low yields. The latter stems through the radical-derived pathways shown in Figure 6. Figure 10c also portrays the increasing trend of the two experimentally detected products, NH_3 and CO_2.

It shall be noted that the constricted model only accounts for purely gas-phase reactions; i.e., the model does not account for reaction in the condensed medium, which could be fundamentally different. The onset of the decomposition of Ser in the gas phase thus requires a significantly higher temperature than that in the condensed phase reported in TGA runs. The model serves to elucidate the fate of evaporated Ser that may form during the pyrolysis of biomass. Building a comprehensive model requires the integration of

https://doi.org/10.1021/acsomega.3c10496
ACS Omega 2024, 9, 8574−8584

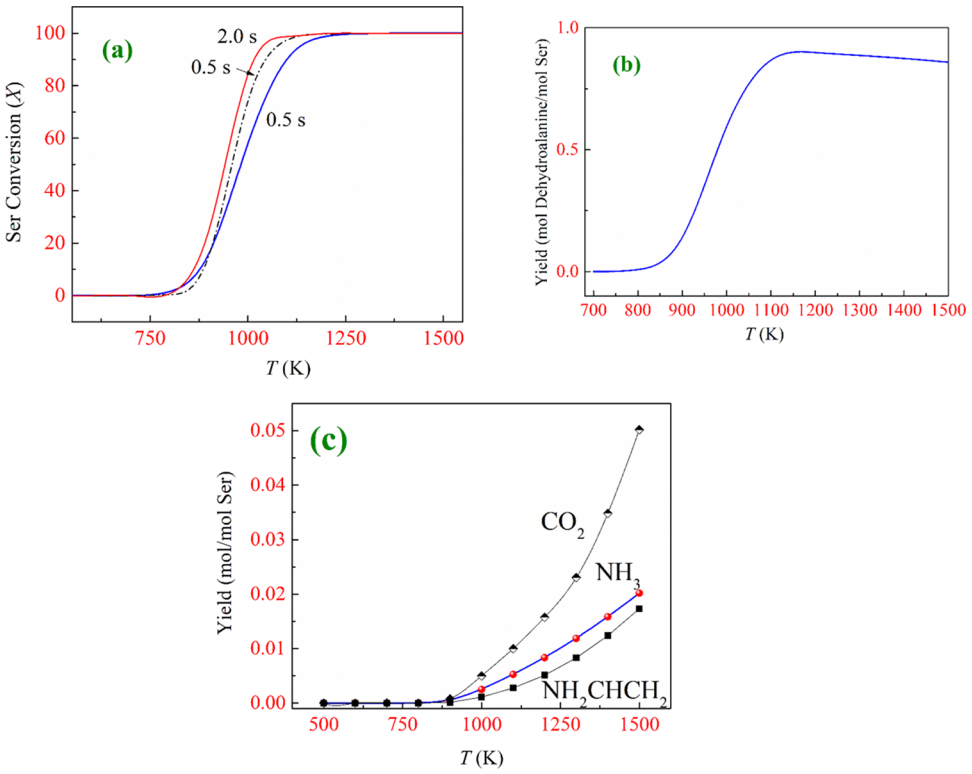

Figure 10. Simulated gas-phase conversion of the serine molecule (a) and yields of the 2-aminoacrylic acid (b) and CO_2/NH_3/NH_2CHCH_2 (c). Inlet conditions: 5% serine and 95% N_2 at a 1 s residence time.

reactions in the condensed medium that are likely to be dominated by cross-linking dehydration and deamination reactions, in addition to the direct expulsion of CO_2, CO, and NH_3. An accurate model is likely to contain thousands of reactions and species; nonetheless, the model presented herein presents likely initiation reactions leading to some of the final observed products. Likewise, heat and mass transfer aspects are expected to play a central role in the fragmentation of the crystalline material.

4. CONCLUSIONS

To comprehend the pyrolysis chemistry of α-amino acids, we presented herein thermokinetic parameters for a large array of reactions that participate in the initial decomposition of the Ser molecule. Attained parameters were utilized to construct a kinetic model to describe the decay of the vapor-phase Ser. The governing steps in the gas phase fundamentally differ from those prevailing in the condensed medium. The latter is controlled by cross-linking reactions, while the former is underpinned by a dehydration reaction. Thus, the degradation mechanism of Ser in the gas phase is decoupled from that in the condensed phase, opposite to the simplified mechanistic overview presented in recent studies. In view of their very high activation energies compared with the water elimination channel, deamination and decarboxylation channels are of negligible importance. The ionic form in the crystalline phase of Ser facilities direct emission of major experimentally detected products, namely, NH_3, CO_2, and CO. A relatively low barrier for a dehydration reaction in the self-condensation of Ser molecules is in accord with the onset temperature reported in TGA runs. The formulated model for the degradation of Ser in the gas phase discloses that the conversion of Ser commences at relatively high temperatures, with the formation of minor amounts of $HCNH_2$ and ethynamine.

■ ASSOCIATED CONTENT

Supporting Information

The Supporting Information is available free of charge at https://pubs.acs.org/doi/10.1021/acsomega.3c10496.

Cartesian coordinates and vibrational frequencies for all structures and thermokinetic parameters in the developed kinetic model (PDF)

■ AUTHOR INFORMATION

Corresponding Author

Mohammednoor Altarawneh − *Department of Chemical and Petroleum Engineering, United Arab Emirates University, Al-Ain 15551, United Arab Emirates;* orcid.org/0000-0002-2832-3886; Email: mn.Altarawneh@uaeu.ac.ae

Authors

Mubarak Al-Kwradi − *Department of Chemical and Petroleum Engineering, United Arab Emirates University, Al-Ain 15551, United Arab Emirates*

Labeeb Ali − *Department of Chemical and Petroleum Engineering, United Arab Emirates University, Al-Ain 15551, United Arab Emirates;* orcid.org/0000-0002-4877-4801

Complete contact information is available at: https://pubs.acs.org/10.1021/acsomega.3c10496

Notes

The authors declare no competing financial interest.

https://doi.org/10.1021/acsomega.3c10496
ACS Omega 2024, 9, 8574−8584

■ ACKNOWLEDGMENTS

This study has been supported by a grant from the National Water and Energy Center at the United Arab Emirates University, UAEU (grant number: 12R124). Computations were carried out at the high-performance computing cluster of the UAEU.

■ ABBREVIATIONS

BDH	bond dissociation enthalpy
CBS-QB3	complete basis set
DFT	density functional theory
A	Arrhenius pre-exponential factor
E_a	energy of activation
ΔH_{f298}^{o}	standard enthalpy of formation
S_{298}^{o}	standard entropy
$Cp\ (T)$	heat capacity at a range of temperatures
PES	potential energy surface
Ser	serine
TGA	thermogravimetric analysis
TST	transition-state theory
P1	radical product for H-abstracted from Ser at the −COOH site
P2	radical product for H-abstracted from Ser at the $-NH_2$ site
P3	radical product for H-abstracted from Ser at the $-\alpha$ CH site
P4	radical product for H-abstracted from Ser at the $-\beta$ CH site (secondary C)
P5	radical product for H-abstracted from Ser at the −OH site
M1	Ser product after dehydration channel process (2-aminoacrylic acid)
M2	Ser product after decarboxylation channel process (monoethanolamine)
M3	Ser product after deamination channel process
M8	bimolecular Ser product through dehydration channel process
M9	bimolecular Ser product after losing NH_3

■ REFERENCES

(1) Ahn, B.; Park, C.; Liu, J. J.; Ok, Y. S.; Won, W. Maximizing the utilization of lignocellulosic biomass: Process development and analysis. *Renewable Energy* **2023**, *215*, No. 119004.

(2) Naqvi, S. A. A.; Hussain, M.; Hussain, B.; Shah, S. A. R.; Nazir, J.; Usman, M. Environmental sustainability and biomass energy consumption through the lens of pollution Haven hypothesis and renewable energy-environmental kuznets curve. *Renewable Energy* **2023**, *212*, 621−631.

(3) Yang, X.; Hou, R.; Fu, Q.; Li, T.; Wang, J.; Su, Z.; Shen, W.; Zhou, W.; Wang, Y. Effect of freeze-thaw cycles and biochar coupling on the soil water-soil environment, nitrogen adsorption and N2O emissions in seasonally frozen regions. *Sci. Total Environ.* **2023**, *893*, No. 164845.

(4) Zhao, J.; Shi, L.; Shi, J.; Li, H.; Lang, D.; Wei, Z.; Li, S.; Pan, B. Distribution of environmentally persistent free radicals in size-segregated PMs emitted from residential biomass fuel combustion. *J. Hazard. Mater.* **2023**, *449*, No. 130956.

(5) Kim, Y.; Thomas, A. E.; Robichaud, D. J.; Iisa, K.; St John, P. C.; Etz, B. D.; Fioroni, G. M.; Dutta, A.; McCormick, R. L.; Mukarakate, C.; Kim, S. A perspective on biomass-derived biofuels: From catalyst design principles to fuel properties. *J. Hazard. Mater.* **2020**, *400*, No. 123198.

(6) Williams, A.; Jones, J. M.; Ma, L.; Pourkashanian, M. Pollutants from the combustion of solid biomass fuels. *Prog. Energy Combust. Sci.* **2012**, *38* (2), 113−137.

(7) Glarborg, P.; Miller, J. A.; Ruscic, B.; Klippenstein, S. J. Modeling nitrogen chemistry in combustion. *Prog. Energy Combust. Sci.* **2018**, *67*, 31−68.

(8) Leng, L.; Yang, L.; Chen, J.; Leng, S.; Li, H.; Li, H.; Yuan, X.; Zhou, W.; Huang, H. A review on pyrolysis of protein-rich biomass: Nitrogen transformation. *Bioresour. Technol.* **2020**, *315*, No. 123801.

(9) Chen, W.; Yang, H.; Chen, Y.; Li, K.; Xia, M.; Chen, H. Influence of biochar addition on nitrogen transformation during copyrolysis of algae and lignocellulosic biomass. *Environ. Sci. Technol.* **2018**, *52* (16), 9514−9521.

(10) Chen, W.; Chen, Y.; Yang, H.; Xia, M.; Li, K.; Chen, X.; Chen, H. Co-pyrolysis of lignocellulosic biomass and microalgae: Products characteristics and interaction effect. *Bioresour. Technol.* **2017**, *245*, 860−868.

(11) Ren, Q.; Zhao, C. NO_x and N_2O precursors from biomass pyrolysis: Nitrogen transformation from amino acid. *Environ. Sci. Technol.* **2012**, *46* (7), 4236−4240.

(12) Ren, Q.; Zhao, C. Evolution of fuel-N in gas phase during biomass pyrolysis. *Renewable Sustainable Energy Rev.* **2015**, *50*, 408−418.

(13) Bhadra, B. N.; Jhung, S. H. Oxidative desulfurization and denitrogenation of fuels using metal-organic framework-based/-derived catalysts. *Appl. Catal., B* **2019**, *259*, No. 118021.

(14) Xu, D.; Lin, J.; Ma, R.; Hou, J.; Sun, S.; Ma, N. Fast pyrolysis of algae model compounds for bio-oil: In-depth insights into the volatile interaction mechanisms based on DFT calculations. *Fuel* **2023**, *333*, No. 126449.

(15) Hao, J.; Guo, J.; Xie, F.; Xia, Q.; Xie, J. Correlation of hydrogen cyanide formation with 2,5-diketopiperazine and nitrogen heterocyclic compounds from co-pyrolysis of glycine and glucose/fructose. *Energy Fuels* **2013**, *27* (8), 4723−4728.

(16) Jabeen, S.; Zeng, Z.; Altarawneh, M.; Gao, X.; Saeed, A.; Dlugogorski, B. Z. Thermal decomposition of model compound of algal biomass. *Int. J. Chem. Kinet.* **2019**, *51* (9), 696−710.

(17) Do, H. T.; Chua, Y. Z.; Kumar, A.; Pabsch, D.; Hallermann, M.; Zaitsau, D.; Schick, C.; Held, C. Melting properties of amino acids and their solubility in water. *RSC Adv.* **2020**, *10* (72), 44205−44215.

(18) Weiss, I. M.; Muth, C.; Drumm, R.; Kirchner, H. O. K. Thermal decomposition of the amino acids glycine, cysteine, aspartic acid, asparagine, glutamic acid, glutamine, arginine and histidine. *BMC Biophys.* **2018**, *11*, No. 2.

(19) Chen, H.; Xie, Y.; Chen, W.; Xia, M.; Li, K.; Chen, Z.; Chen, Y.; Yang, H. Investigation on co-pyrolysis of lignocellulosic biomass and amino acids using TG-FTIR and Py-GC/MS. *Energy Convers. Manage.* **2019**, *196*, 320−329.

(20) Chen, P.; Gong, M.; Chen, Y.; Zhou, Z.; Liu, M.; Fang, Y.; Chen, W.; Yang, H.; Chen, H. Thermal decomposition pathways of phenylalanine and glutamic acid and the interaction mechanism between the two amino acids and glucose. *Fuel* **2022**, *324*, No. 124345.

(21) Xu, D.; Lin, J.; Sun, S.; Ma, R.; Wang, M.; Yang, J.; Luo, J. Microwave pyrolysis of biomass model compounds for bio-oil: Formation mechanisms of the nitrogenous chemicals and DFT calculations. *Energy Convers. Manage.* **2022**, *262*, No. 115676.

(22) Lund, M. N.; Ray, C. A. Control of Maillard reactions in foods: Strategies and chemical mechanisms. *J. Agric. Food Chem.* **2017**, *65* (23), 4537−4552.

(23) Sato, N.; Quitain, A. T.; Kang, K.; Daimon, H.; Fujie, K. Reaction kinetics of amino acid decomposition in high-temperature and high-pressure water. *Ind. Eng. Chem. Res.* **2004**, *43* (13), 3217−3222.

(24) Frisch, M. J.; Trucks, G. W.; Schlegel, H. B.; Scuseria, G. E.; Robb, M. A.; Cheeseman, J. R.; Scalmani, G.; Barone, V.; Petersson, G. A.; Nakatsuji, H.; Li, X.; Caricato, M.; Marenich, A. V.; Bloino, J.; Janesko, B. G.; Gomperts, R.; Mennucci, B.; Hratchian, H. P.; Ortiz, J. V.; Izmaylov, A. F.; Sonnenberg, J. L.; Williams; Ding, F.; Lipparini,

https://doi.org/10.1021/acsomega.3c10496
ACS Omega 2024, 9, 8574−8584

F.; Egidi, F.; Goings, J.; Peng, B.; Petrone, A.; Henderson, T.; Ranasinghe, D.; Zakrzewski, V. G.; Gao, J.; Rega, N.; Zheng, G.; Liang, W.; Hada, M.; Ehara, M.; Toyota, K.; Fukuda, R.; Hasegawa, J.; Ishida, M.; Nakajima, T.; Honda, Y.; Kitao, O.; Nakai, H.; Vreven, T.; Throssell, K.; Montgomery, J. A., Jr.; Peralta, J. E.; Ogliaro, F.; Bearpark, M. J.; Heyd, J. J.; Brothers, E. N.; Kudin, K. N.; Staroverov, V. N.; Keith, T. A.; Kobayashi, R.; Normand, J.; Raghavachari, K.; Rendell, A. P.; Burant, J. C.; Iyengar, S. S.; Tomasi, J.; Cossi, M.; Millam, J. M.; Klene, M.; Adamo, C.; Cammi, R.; Ochterski, J. W.; Martin, R. L.; Morokuma, K.; Farkas, O.; Foresman, J. B.; Fox, D. J. *Gaussian 16*, Rev. C.01; Wallingford, CT, 2016.

(25) Montgomery, J. A., Jr.; Frisch, M. J.; Ochterski, J. W.; Petersson, G. A. A complete basis set model chemistry. VI. Use of density functional geometries and frequencies. *J. Chem. Phys.* **1999**, *110* (6), 2822−2827.

(26) Rahman, R. K.; Arafin, F.; Neupane, S.; Wang, C.-H.; Baker, J.; Ninnemann, E.; Masunov, A. E.; Vasu, S. S. High-temperature pyrolysis experiments and chemical kinetics of diisopropyl methylphosphonate (DIMP), a simulant for Sarin. *Combust. Flame* **2022**, *245*, No. 112345.

(27) Matsugi, A.; Suzuki, S. Multiple-well master equation study on the propargyl + indenyl recombination and subsequent reactions. *Combust. Flame* **2024**, *259*, No. 113143.

(28) Siddique, K.; Altarawneh, M.; Gore, J.; Westmoreland, P. R.; Dlugogorski, B. Z. Hydrogen abstraction from hydrocarbons by NH_2. *J. Phys. Chem. A* **2017**, *121* (11), 2221−2231.

(29) Rawadieh, S. E.; Altarawneh, M.; Altarawneh, I. S.; Shiroudi, A.; El-Nahas, A. M. Exploring reactions of amines-model compounds with NH_2: In relevance to nitrogen conversion chemistry in biomass. *Fuel* **2021**, *291*, No. 120076.

(30) Somers, K. P.; Simmie, J. M. Benchmarking Compound Methods (CBS-QB3, CBS-APNO, G3, G4, W1BD) against the Active Thermochemical Tables: Formation Enthalpies of Radicals. *J. Phys. Chem. A* **2015**, *119* (33), 8922−8933.

(31) Canneaux, S.; Bohr, F.; Henon, E. KiSThelP: A program to predict thermodynamic properties and rate constants from quantum chemistry results†. *J. Comput. Chem.* **2014**, *35* (1), 82−93.

(32) Mokrushin, V.; Bedanov, V.; Tsang, W.; Zachariah, M. R.; Knyazev, V. D.; McGivern, S. *ChemRate*, 1.5.10 NIST: 2011.

(33) Kundrat, M. D.; Autschbach, J. Computational Modeling of the Optical Rotation of Amino Acids: A New Look at an Old Rule for pH Dependence of Optical Rotation. *J. Am. Chem. Soc.* **2008**, *130* (13), 4404−4414.

(34) McClurg, R. B.; Flagan, R. C.; Goddard Iii, W. A. The hindered rotor density-of-states interpolation function. *J. Chem. Phys.* **1997**, *106* (16), 6675−6680.

(35) Di Giacomo, F. A Short Account of RRKM theory of unimolecular reactions and of marcus theory of electron transfer in a historical perspective. *J. Chem. Educ.* **2015**, *92* (3), 476−481.

(36) Clark, S. J.; Segall, M. D.; Pickard, C. J.; Hasnip, P. J.; Probert, M. I. J.; Refson, K.; Payne, M. C. First principles methods using CASTEP. *Z. Kristallogr. - Cryst. Mater.* **2005**, *220* (5−6), 567−570.

(37) Perdew, J. P.; Burke, K.; Ernzerhof, M. Generalized gradient approximation made simple. *Phys. Rev. Lett.* **1996**, *77* (18), 3865−3868.

(38) Altarawneh, M.; Almatarneh, M. H.; Dlugogorski, B. Z. Thermal decomposition of perfluorinated carboxylic acids: Kinetic model and theoretical requirements for PFAS incineration. *Chemosphere* **2022**, *286*, No. 131685.

(39) Altarawneh, M. Temperature-dependent profiles of dioxin-like toxicants from combustion of brominated flame retardants. *H. Hazard. Mater.* **2022**, *422*, No. 126879.

(40) Altarawneh, I. S.; Altarawneh, M.; Rawadieh, S. E.; Almatarneh, M. H.; Shiroudi, A.; El-Nahas, A. M. Updated yields of nitrogenated species in flames of ammonia/benzene via introducing an aniline submechanism. *Combust. Flame* **2021**, *228*, 433−442.

(41) Altarawneh, M.; Ahmed, O. H.; Al-Harahsheh, M.; Jiang, Z.-T.; Dlugogorski, B. Z. A kinetic model for halogenation of the zinc content in franklinite. *Appl. Surf. Sci.* **2021**, *562*, No. 150105.

(42) Linstrom, P. J.; Mallard, W. G. The NIST Chemistry WebBook: A Chemical Data Resource on the Internet. *J. Chem. Eng. Data* **2001**, *46* (5), 1059−1063.

(43) Chase, M. W., Jr. NIST-JANAF Themochemical Tables, Fourth Edition. *J. Phys. Chem. Ref. Data, Monogr.* **1998**, *9*, 1−1951.

(44) G, J. H. S. Thermodynamic properties of organic oxygen compounds. Part 5. Ethyl alcohol. *Trans. Faraday Soc.* **1962**, *57*, 2132−2137.

(45) Ngauv, S. N.; Sabbah, R.; Laffitte, M. Thermodynamique de composes azotes. III. Etude thermochimique de la glycine et de la l-α-alanine. *Thermochim. Acta* **1977**, *20*, 371−380, DOI: 10.1016/0040-6031(77)85091-0.

(46) Nunes, C. M.; Lapinski, L.; Fausto, R.; Reva, I. Near-IR laser generation of a high-energy conformer of L-alanine and the mechanism of its decay in a low-temperature nitrogen matrix. *J. Chem. Phys.* **2013**, *138*, No. 125101.

(47) Al-Kwradi, M.; Ali, L.; Altarawneh, M. Kinetic parameters for H abstraction from the serine amino acid molecule. *Comput. Theor. Chem.* **2023**, *1225*, No. 114176.

(48) Vistoli, G.; De Maddis, D.; Cipak, A.; Zarkovic, N.; Carini, M.; Aldini, G. Advanced glycoxidation and lipoxidation end products (AGEs and ALEs): an overview of their mechanisms of formation. *Free Radical Res.* **2013**, *47* (sup1), 3−27.

(49) Nakayoshi, T.; Kato, K.; Kurimoto, E.; Oda, A. Possible mechanisms of nonenzymatic formation of dehydroalanine residue catalyzed by dihydrogen phosphate ion. *J. Phys. Chem. B* **2019**, *123* (15), 3147−3155.

(50) Körner, P. Hydrothermal degradation of amino acids. *ChemSusChem* **2021**, *14* (22), 4947−4957.

(51) Licht, O.; Barreiro-Lage, D.; Rousseau, P.; Giuliani, A.; Milosavljević, A. R.; Isaak, A.; Mastai, Y.; Albeck, A.; Singh, R.; Nguyen, V. T. T.; Nahon, L.; Martínez-Fernández, L.; Díaz-Tendero, S.; Toker, Y. Peptide Bond Formation in the Protonated Serine Dimer Following Vacuum UV Photon-Induced Excitation. *Angew. Chem., Int. Ed.* **2023**, *62* (15), No. e202218770.

(52) Barreiro-Lage, D.; Chiarinelli, J.; Bolognesi, P.; Richter, R.; Zettergren, H.; Stockett, M. H.; Díaz-Tendero, S.; Avaldi, L. Photofragmentation specificity of photoionized cyclic amino acids (diketopiperazines) as precursors of peptide building blocks. *Phys. Chem. Chem. Phys.* **2023**, *25* (23), 15635−15646.

(53) Rousseau, P.; Piekarski, D. G.; Capron, M.; Domaracka, A.; Adoui, L.; Martín, F.; Alcamí, M.; Díaz-Tendero, S.; Huber, B. A. Polypeptide formation in clusters of β-alanine amino acids by single ion impact. *Nat. Commun.* **2020**, *11* (1), No. 3818.

(54) Aguilar-Pineda, J. A.; Méndez-Maldonado, G. A.; Núñez-Rojas, E.; Alejandre, J. Parametrisation of a force field of acetamide for simulations of the liquid phase. *Mol. Phys.* **2015**, *113* (17−18), 2716−2724.

(55) Bursch, M.; Mewes, J.-M.; Hansen, A.; Grimme, S. Best-Practice DFT Protocols for Basic Molecular Computational Chemistry**. *Angew. Chem., Int. Ed.* **2022**, *61* (42), No. e202205735.

(56) Xiao, F.; Sun, X.; Li, Z.; Li, X. Theoretical Study of Radical−Molecule Reactions with Negative Activation Energies in Combustion: Hydroxyl Radical Addition to Alkenes. *ACS Omega* **2020**, *5* (22), 12777−12788.

(57) Rappsilber, J. The beginning of a beautiful friendship: Cross-linking/mass spectrometry and modelling of proteins and multi-protein complexes. *J. Struct. Biol.* **2011**, *173* (3), 530−540.

(58) Moggach, S. A.; Allan, D. R.; Morrison, C. A.; Parsons, S.; Sawyer, L. Effect of pressure on the crystal structure of L-serine-I and the crystal structure of L-serine-II at 5.4 GPa. *Acta Crystallogr., Sect. B: Struct. Sci.* **2005**, *61*, 58−68.

https://doi.org/10.1021/acsomega.3c10496
ACS Omega 2024, 9, 8574−8584